Cellular and Molecular Life Sciences (2024) 81:429
https://doi.org/10.1007/s00018-024-05462-2



ORIGINAL ARTICLE

# Silencing of maternally expressed RNAs in *Dlk1-Dio3* domain causes fatal vascular injury in the fetal liver

**Haoran Yu[1] · Yue Zhao[2] · Rui Cheng[3] · Mengyun Wang[1] · Xin Hu[1] · Ximeijia Zhang[1] · Xiangqi Teng[1] · Hongjuan He[1] · Zhengbin Han[4] · Xiao Han[1] · Ziwen Wang[1] · Bingjing Liu[1] · Yan Zhang[5] · Qiong Wu[1]**

Received: 12 June 2024 / Revised: 20 September 2024 / Accepted: 25 September 2024


## Abstract

The mammalian imprinted *Dlk1-Dio3* domain contains multiple lncRNAs, mRNAs, the largest miRNA cluster in the genome and four differentially methylated regions (DMRs), and deletion of maternally expressed RNA within this locus results in embryonic lethality, but the mechanism by which this occurs is not clear. Here, we optimized the model of maternally expressed RNAs transcription termination in the domain and found that the cause of embryonic death was apoptosis in the embryo, particularly in the liver. We generated a mouse model of maternally expressed RNAs silencing in the *Dlk1-Dio3* domain by inserting a 3 × polyA termination sequence into the *Gtl2* locus. By analyzing RNA-seq data of mouse embryos combined with histological analysis, we found that silencing of maternally expressed RNAs in the domain activated apoptosis, causing vascular rupture of the fetal liver, resulting in hemorrhage and injury. Mechanistically, termination of *Gtl2* transcription results in the silencing of maternally expressed RNAs and activation of paternally expressed genes in the interval, and it is the gene itself rather than the IG-DMR and *Gtl2*-DMR that causes the aforementioned phenotypes. In conclusion, these findings illuminate a novel mechanism by which the silencing of maternally expressed RNAs within *Dlk1-Dio3* domain leads to hepatic hemorrhage and embryonic death through the activation of apoptosis.

**Keywords** Long non-coding RNAs · Easi-CRISPR · Maternally expressed RNAs · Embryonic lethality · Mouse

## Introduction

Genomic imprinting is a unique epigenetic regulation that results in parent-specific gene expression and is essential for normal development and growth in mammals [1, 2]. As an important genomic region, the genes and elements in the *Dlk1-Dio3* imprinting region play a key role in embryonic development, cell differentiation and disease occurrence [3, 4]. The study of this region provides insights into the mechanisms of genomic imprinting and the functions of imprinted genes in organism development and disease.

The long non-coding RNA (lncRNA) gene trap locus 2 (*Gtl2*), which is known as maternally expressed gene 3 (*MEG3*) in humans and has an imprinting pattern of maternal expression and paternal imprinting, is an imprinting gene located in the *Dlk1-Dio3* imprinting gene cluster [5]. Downstream maternally expressed intergenic transcripts are transcribed in the same direction as those of *Gtl2*, and canonical promoter sequences are apparently absent from this region, with all lncRNAs regulated by common *cis*-elements and epigenetic control to produce a large polycistronic

✉ Yan Zhang
zhangtyo@hit.edu.cn

✉ Qiong Wu
kigo@hit.edu.cn

1 School of Life Science and Technology, State Key Laboratory of Urban Water Resource and Environment, Harbin Institute of Technology, Harbin 150001, China

2 Department of Urology, School of Medicine, Xiang'an Hospital of Xiamen University, Xiamen University, Xiamen 361000, China

3 State Key Laboratory for Conservation and Utilization of Bio-Resource and School of Life Sciences, Yunnan University, Kunming 650091, China

4 HIT Center for Life Sciences, School of Life Science and Technology, Harbin Institute of Technology, Harbin 150001, China

5 Computational Biology Research Center, School of Life Science and Technology, Harbin Institute of Technology, Harbin 150001, China

Published online: 09 October 2024

transcription unit [6]. Furthermore, the tissue-specific features of *Gtl2* and these microRNAs (miRNAs) are strikingly similar, suggesting coordinated regulation of the expression of these genes [7–9]. Three studies have shown that *Gtl2* knockout causes death of mouse. But curiously, the lethal genotypes and phenotypes of mice in these studies were different, and some were even contradictory.

When the 9.8 kb region of *Gtl2*-DMR and exon 1–5 was knocked out, the maternal knockout mice were born normally, but all died within 4 weeks, while the paternal knockout mice showed growth retardation and perinatal mortality, meanwhile, the homozygous knockout mice could survive normally [10]. Another study also knocked out a 5.9 kb fragment in the similar region of *Gtl2*, but the results were completely different: maternal and homozygous knockout mice resulted in perinatal death, while paternal knockout mice were born and developed normally [11]. By constructing mouse models with deletion of *Meg3* 1–4 exon ($Meg3^{\Delta 1-4}$) and deleton of *Meg3* 2–4 exon deletion ($Meg3^{\Delta 2-4}$), it was found that maternal $Meg3^{\Delta 1-4}$ caused the death of embryos at embryonic day 13.5 (E13.5), and the maternal $Meg3^{\Delta 2-4}$ mice were able to be born normally, however, the data information of homozygous double deletion in parents was missing [12]. Although these three reports all focused on *Gtl2* gene knockout, the conclusions obtained were not mutually corroborative and even contradictory. After comparing the three reported gene knockout regions, it was found that the large knockout gene may lead to the deletion of miRNAs, *Gtl2*-DMR and genomic regulatory elements within the *Gtl2* gene, or interfere with the active open chromatin region in the *Gtl2* locus, so the obtained experimental results did not reflect the true role of *Gtl2*. In addition, several articles have pointed out that gene knockout is not suitable for the study of lncRNA function, which may cause false positive results [13, 14]. Therefore, a new method that can accurately describe the function of lncRNA is urgently needed.

The mammalian fetal liver can not only participate in glucose and lipid metabolism, but also synthesize substances such as hemoglobin, coagulation factors and bilirubin [15–19]. Meanwhile, as a major hematopoietic organ, the fetal liver provides the embryo with essential erythrocytes and other blood components [20, 21]. In addition, when the blood vessels of fetal liver are damaged and hemorrhage occurs, it will cause serious consequences such as liver damage, abdominal hemorrhage, embryonic development restriction and even death [22, 23]. Previous studies have mainly explored the role of fetal liver in metabolism, hematopoiesis and regeneration, but lack of exploration of liver vascular development. There is a close relationship between *Dlk1-Dio3* domain and the fetal liver. Previous studies have described that the gene expression in this region has an important impact on the metabolism and hematopoietic functions of the fetal liver [20, 21, 24], but the description of the development of the liver vascular system is lacking.

In this study, the Easi-CRISPR strategy was used to successfully establish *Gtl2* transcription termination mice model by inserting 3 × polyA termination sequence [25]. Our previous studies have reported the importance of this domain for placental vasculature [25]. Subsequently, we observed that silencing of maternally expressed RNAs in *Dlk1-Dio3* domain resulted in embryonic lethality due to liver vascular damage, fatal hepatic hemorrhage in mice. Precise gene expression analysis showed that after *Gtl2* transcription termination, maternally expressed RNAs in the *Dlk1-Dio3* domain were almost completely silenced, while paternally expressed genes were activated. Together, this study explained that silencing of maternally expressed RNAs in *Dlk1-Dio3* domain caused apoptosis in embryo, especially in liver, leading to vascular damage, causing large area of liver hemorrhage and embryonic death.

## Materials and methods

### Animals

We improved and optimized the Easi-CRISPR gene knock-in method [26]. According to the prediction analysis of the websites ((http://crispr.wustl.edu/ and http://www.rgenome.net/cas-designer/), we found an efficient sgRNA after *Gtl2* promoter, formed RNP complex with Cas9 protein and gRNA, and then microinjected the fertilized male pronucleus together with ssDNA, and efficiently established the mouse model of transcription termination of maternally expressed RNA in *Dlk1-Dio3* domain. $Gtl2^{+/+}$ female mice were mated with $Gtl2^{+/polyA}$ male mice for propagation and expansion of the system. Male and female mice were mated at 6:00p.m. and vaginal suppositories were tested at 9:00a.m., the next day, and the presence of vaginal plugs was marked as E0.5. B6D2F1 (BDF1) female mice were induced to superovulate, and the superovulated females were mated with BDF1 male mice for zygote collection. The initial pronuclear injection was performed in these zygotes. The SNP site on the *Dlk1* locus could distinguish whether the newborn mice were of C57BL/6N or DBA/2J background, and finally one male mouse of C57BL/6N and DBA/2J background was selected as founder mice of the two strains for subsequent experiments. The mice used for biallelic expression and methylation analysis were derived from the hybrid offspring of DBA/2J and C57BL/6N strains, while the remaining experimental strains in this study were all from DBA/2J mice. Wide-type DBA/2J and C57BL/6N mice were purchased from Beijing, Weitonglihua.

## RNA-seq analysis

We selected one sample from each of the four genotypes and extracted 1 μg of total RNA, and the cDNA library was generated and sequenced on Illumina sequencing platform provided by Biomarker technologies (Wuhan, China) (www.biomarker.com.cn). We used FASTQ to assess the quality of sequencing data, and poor-quality reads were removed. We selected mouse GRCm38/mm10 as the reference genome, and relied on several comprehensive databases such as Ensembl (https://asia.ensembl.org/index.html) and GENCODE (https://www.gencodegenes.org/) to identify and annotate mRNAs and lncRNAs. Then, we compared high-quality reads to the reference genome by HISAT2 [27], quantified reads by StringTie [28], and finally calculated the expression level of each mRNA and lncRNA (FPKM). Differentially expressed lncRNAs, miRNAs and mRNAs were screened were screened by EdgeR [29], with fold change more than 2.0, and p-value less than 0.05. Target genes of lncRNAs were predicted by its *cis*-interaction and *trans*-interaction [30, 31]. Ensembl and UCSC Genome Browser (https://www.genome.ucsc.edu/) were used to identify neighboring genes within 1Mbps of lncRNAs as their *cis*-target genes. And ENCORI (https://rnasysu.com/encori/index.php) were used to predict the *trans*-target genes of lncRNAs. And based on the complementary pairing principle of mRNA 3′UTR [32], we predicted the target genes of miRNAs by miRbase (http://mirbase.org) and Targetscan (https://www.targetscan.org/). Database for Annotation, Visualization and Integrated Discovery (DAVID, https://david.ncifcrf.gov/) and Metascape (https://metascape.org/) were used to analyze the potential functions of target genes of lncRNAs and miRNAs, and mRNA in KEGG pathway and Go terms.

## qRT-PCR analysis

Total RNA was extracted from brain, heart, liver, lung, muscle and embryo at E12.5. cDNA of mRNA and lncRNA were synthesized by using PrimeScript™ RT reagent Kit (TakaRa, RR047Q) in a 10 μl reaction solution containing 500 ng total RNA. cDNA of miRNA was synthesized by using Mir-X™ miRNA First-Strand Synthesis (TakaRa) in a 10 μl reaction solution containing 500 ng total RNA. The gene expression levels were measured by real-time PCR with the SYBR Green PCR Master Mix. *β-Actin* was used as control for mRNA and lncRNA. *U6* was used as control for miRNA. Values from wild-type were designated as 1. Values from $Gtl2^{+/polyA}$, $Gtl2^{polyA/+}$ and $Gtl2^{polyA/polyA}$ were normalized against those from $Gtl2^{+/+}$. Primers' sequences were shown in Tab. S1.

## Biallelic expression of Dlk1

Chromosome-specific gene expression was determined by SNP analysis. In *Dlk1* cDNA (NM_010052), SNP is a G in C57BL/6N and an A in DBA/2J, respectively. Total RNA was isolated from E12.5 embryos obtained by crossing $Gtl2^{+/+}$ DBA/2J with $Gtl2^{+/polyA}$ C57BL/6N mice and crossing $Gtl2^{+/polyA}$ DBA/2J with $Gtl2^{+/+}$ C57BL/6N mice. The region containing the polymorphism was amplified by RT-PCR. The allelic expression of *Dlk1* was determined by sequencing PCR products. Primers' sequences were shown in Tab. S1.

## DNA methylation analysis

Genomic DNAs were isolated from E12.5 embryos (DBA/2J x C57BL/6N). After bisulfite treatment by EZ DNA Methylation-Gold™ kit (Zymo Research), the converted genomic DNAs were amplified by PCR for *Gtl2*-DMR and IG-DMR, which primers' sequences were shown in Tab. S1 Results were read by DNAMAN Version 6 after sequencing (Comate Bioscience, China). Primers' sequences were shown in Tab. S1.

## Histologyical analysis

Fetal livers of E12.5 were fixed with 4% paraformaldehyde of 24 h, dehydrated with ethanol and transparent with xylene, then paraffin blocks were prepared, sliced 5 μm and stained with hematoxylin/eosin. Images were captured with Zeiss optical microscope (Germany).

## Vascular area analysis

We regarded the closed interval surrounded by CD31 signal as one vessel, and quantified the area of the enclosed vessel by imageJ. Within a view, the average vessel area per unit area is obtained by (total vessel area / total number) /view area.

## Preparation of blood smears

Peripheral blood of mouse embryos at E12.5 were taken to make blood pictures and stained with Wright-Giemsa Stain kit (Solarbio, G1021). Images were captured with Zeiss optical microscope (Germany).

## Immunohistochemistry

Fetal livers of E12.5 were fixed with 4% paraformaldehyde of 24 h. After blocking with 2% BSA/PBS, sections were incubated with specific primary antibodies at 4 ℃ overnight, and sections were treated with HRP-conjugated secondary

antibodies. DAB kit (ZSGB-BIO, China) was used for chemical staining.

### Assay of Caspase 9 activity

The Caspase 9 spectrophotometric assay kit is based on the combination of a Caspase 9 sequence-specific peptide (acetyl-Asp-Glu-Val-Asp p-nitroanilide, Ac-LEHD-pNA) coupled to the yellow luminescent group p-nitroaniline (pNA). When the substrate was cleaved by Caspase 9, the yellow luminescent group pNA was free, and its absorbance value could be measured by a microplate reader or a spectrophotometer ($\lambda = 405$ nm). Embryo or liver tissue was taken in a petri dish, cut into pieces, added with lysate (400ul/100 mg), homogenized with a glass homogenizer on ice, left in an ice bath for 5 min, and centrifuged. The supernatant was sucked into a new EP tube. After Ac-LEHD-pNA was added and mixed, the mixture was incubated at 37 °C for 2 to 4 h, and OD405 could be determined when the color change was obvious. Finally, the activation degree of Caspase 9 is determined by calculating the multiple of $(OD_{\text{sample value}}\text{-}OD_{\text{blank control}})/(OD_{\text{negative value}}\text{-}OD_{\text{blank control}})$ (Elabscience, E-CK-A313).

### TUNEL apoptosis assay

TUNEL apoptosis assay was detected using frozen sections of fetal liver at E12.5. After fixing with paraformaldehyde, and washing with PBS solution, the assay was used by one step TUNEL Apoptosis Assay kit (Beyotime, C1088). Images were captured with Olympus fluorescence inverted microscope (Japan).

### In situ *hybridization*

Paraffin sections were made as described above. Sections were treated with 2 mg/ml proteinase K in PBS and terminated wit 1 mg/mL glycine. Antisense riboprobes were used for hybridization overnight at 65 °C, alkaline phosphatase-conjugated anti-DIG antibody (Roche, 54,732,420, dilution 1:5000) was incubated overnight at 4 °C, and NBT/BCIP Stock Solution (Roche, 11,681,451,001) was used for chemical staining. Images were captured with Zeiss optical microscopy. Primers' sequences of probe were shown in Tab. S1.

### Statistics

Values are shown as the mean ± SEM as indicated. All statistical analyses were generated using GraphPad Prism 6. Student's t test was used for comparisons between two groups. Statistical significance was defined as $p$ value of $< 0.05$ (*, $p < 0.05$; **, $p < 0.01$; ***, $p < 0.001$).

## Results

### Establishment and genetic analysis of Gtl2 transcription termination mouse

*Gtl2* is located within the *Dlk1-Dio3* imprinting domain at the end of mouse chromosome 12 (Fig. 1a). Previous analysis of the *Gtl2* locus has revealed a differentially methylated region (*Gtl2*-DMR), a microRNA (miR-1906), two CTCF binding sites and some active open chromatin regions between exons 1–5 [12, 33]. In order to silence the *Gtl2* gene without affecting the action and activity of other transcription factors, we identified a highly efficient sgRNA site at the end of the first exon, and used 96 bp of each upstream and downstream sgRNA as the left and right homology arms to form ssDNA with the inserted 3 × polyA (Fig. 1b and c). The combined ssDNA and RNP complex (sgRNA and Cas9 protein) were microinjected into the male pronucleus of the zygote (Fig. S1a), cultured in vitro until the blastocyst stage (Fig. S1b), and the embryos were transferred into two surrogate mice [25]. Among the six newborn mice (Fig. S1c), five founder mice with successful 3 × polyA knock-in were identified by PCR (Fig. 1b and S1d). Taken, we successfully generated a mutant mouse model that only silenced the expression of ncRNA in *Dlk1-Dio3* domain without deleting other active elements.

Since *Gtl2* is a maternally expressed gene, we maintained the generated mice by crossing wild type ($Gtl2^{+/+}$) or *Gtl2* transcription termination occurs on the paternal alleles ($Gtl2^{+/polyA}$) of male mice with $Gtl2^{+/+}$ or $Gtl2^{+/polyA}$ females (Fig. S1e). We selected 3–4 generations of mice for the parents of embryos obtained. Mice developed normally in $Gtl2^{+/polyA}$ mice, while embryonic death began at E13.5 and all mice died at E16.5 (Fig. 1e) when *Gtl2* transcription termination occurred on the maternal allele ($Gtl2^{polyA/+}$) and the homozygous biallelic ($Gtl2^{polyA/polyA}$) (Fig. S1f). The mortality rate of $Gtl2^{polyA/+}$ was 0%, 21.43%, 47.06%, 77.78% and 100% from E12.5 to E16.5, respectively, and then the mortality rate of $Gtl2^{polyA/polyA}$ was 0%, 0%, 58.06%, 100% and 100% form E12.5 to E16.5, respectively (Fig. 1d and S1g). So far, we have found that there is a slight difference in the time of death between $Gtl2^{polyA/+}$ and $Gtl2^{polyA/polyA}$. According to the representative images of embryos, we observed that there was no significant difference in the four-genotype embryos at E12.5. There was no obvious change in $Gtl2^{+/polyA}$, however, the $Gtl2^{polyA/+}$ and $Gtl2^{polyA/polyA}$ mice showed abdominal hemorrhage at E14.5 (Fig. 1e). There was no obvious change in $Gtl2^{+/polyA}$ at E16.5, whereas the $Gtl2^{polyA/+}$ and $Gtl2^{polyA/polyA}$ mice were all dead at this stage (Fig. 1e). $Gtl2^{polyA/+}$ and $Gtl2^{polyA/polyA}$ were slightly

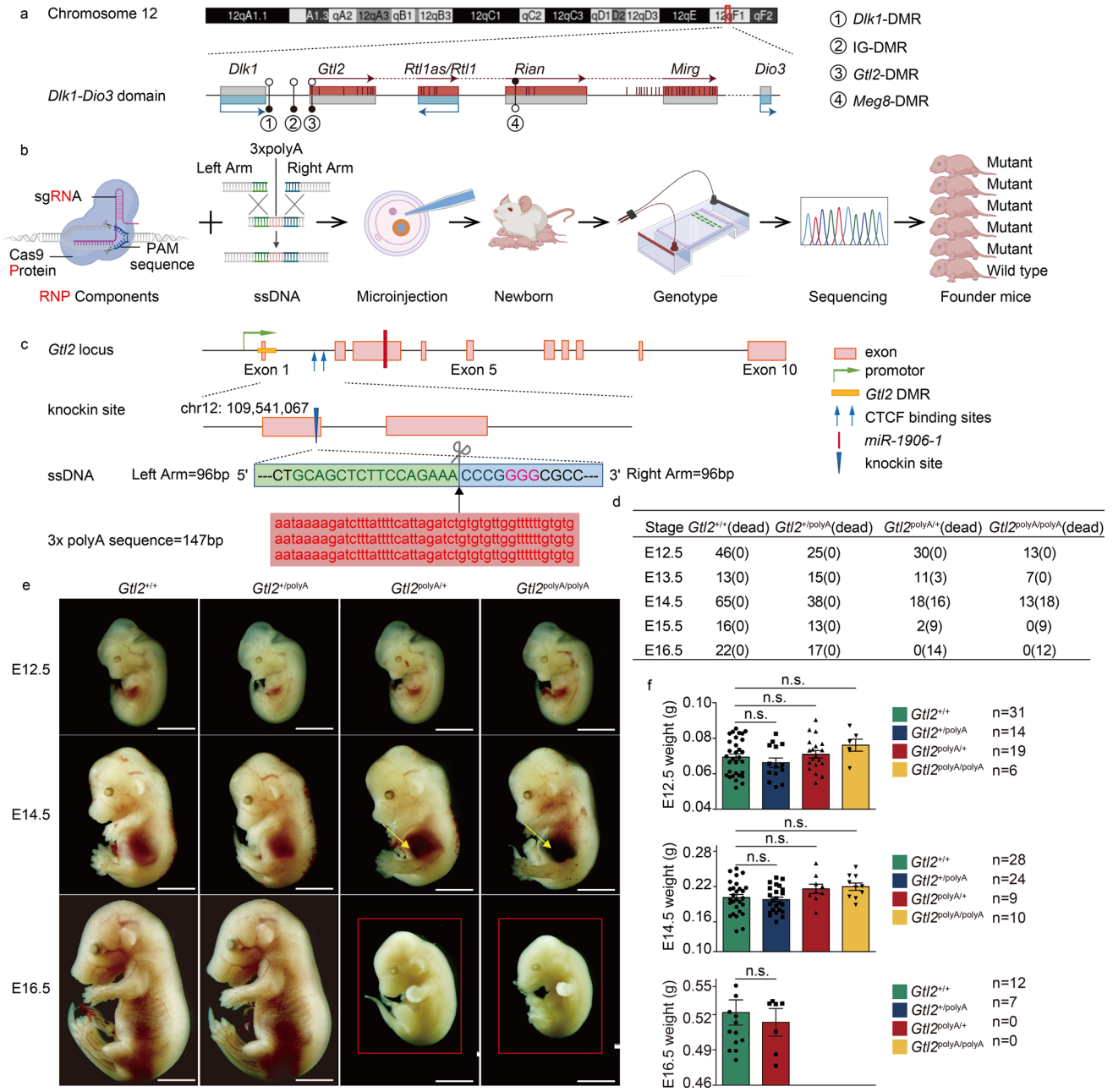


| Stage | $Gtl2^{+/+}$(dead) | $Gtl2^{+/polyA}$(dead) | $Gtl2^{polyA/+}$(dead) | $Gtl2^{polyA/polyA}$(dead) |
|---|---|---|---|---|
| E12.5 | 46(0) | 25(0) | 30(0) | 13(0) |
| E13.5 | 13(0) | 15(0) | 11(3) | 7(0) |
| E14.5 | 65(0) | 38(0) | 18(16) | 13(18) |
| E15.5 | 16(0) | 13(0) | 2(9) | 0(9) |
| E16.5 | 22(0) | 17(0) | 0(14) | 0(12) |

**Fig. 1** Generation and phenotypic analysis of founder mice. **a** Schematic representation of *Dlk1-Dio3* domain in chromosome12. Maternally expressed genes are in red, paternally expressed genes are in blue and silenced genes are in gray, miRNAs are shown as short vertical lines, differentially methylated regions are shown as circles. Filled circle, methylated; open circle, unmethylated. **b** Schematic representation of mutant mouse production by Easi-CRISPR: preparation of RNP components and ssDNA, microinjection, generation of founder offspring, PCR genotyping and off-target detection and obtaining of founder mice. **c** Schematic representation of 3×polyA termination sequence insertion sites. **d** Survival and death number of embryos from E12.5 to E16.5. **e** Representative pictures of embryo at E12.5, E14.5 and E16.5, abdominal hemorrhage are indicated by yellow arrows, dead embryos are in red boxes. Scale bar, 2 mm. **f** Bar chat showing embryo weight of E12.5, E14.5 and E16.5, each dot represents an embryo. Error bars, ± SEM, n.s., $p > 0.05$

but not significantly heavier than $Gtl2^{+/+}$, and $Gtl2^{+/polyA}$ was almost the same compared to $Gtl2^{+/+}$, and the trends of embryo weight change were the same at E12.5, E14.5 and E16.5 (Fig. 1f). Together, these data show that the silencing of ncRNAs on *Dlk1-Dio3* domain results in little effect on $Gtl2^{+/polyA}$, and a slight increase in embryo weight, abdominal hemorrhage and embryonic death on $Gtl2^{polyA/+}$ and $Gtl2^{polyA/polyA}$.

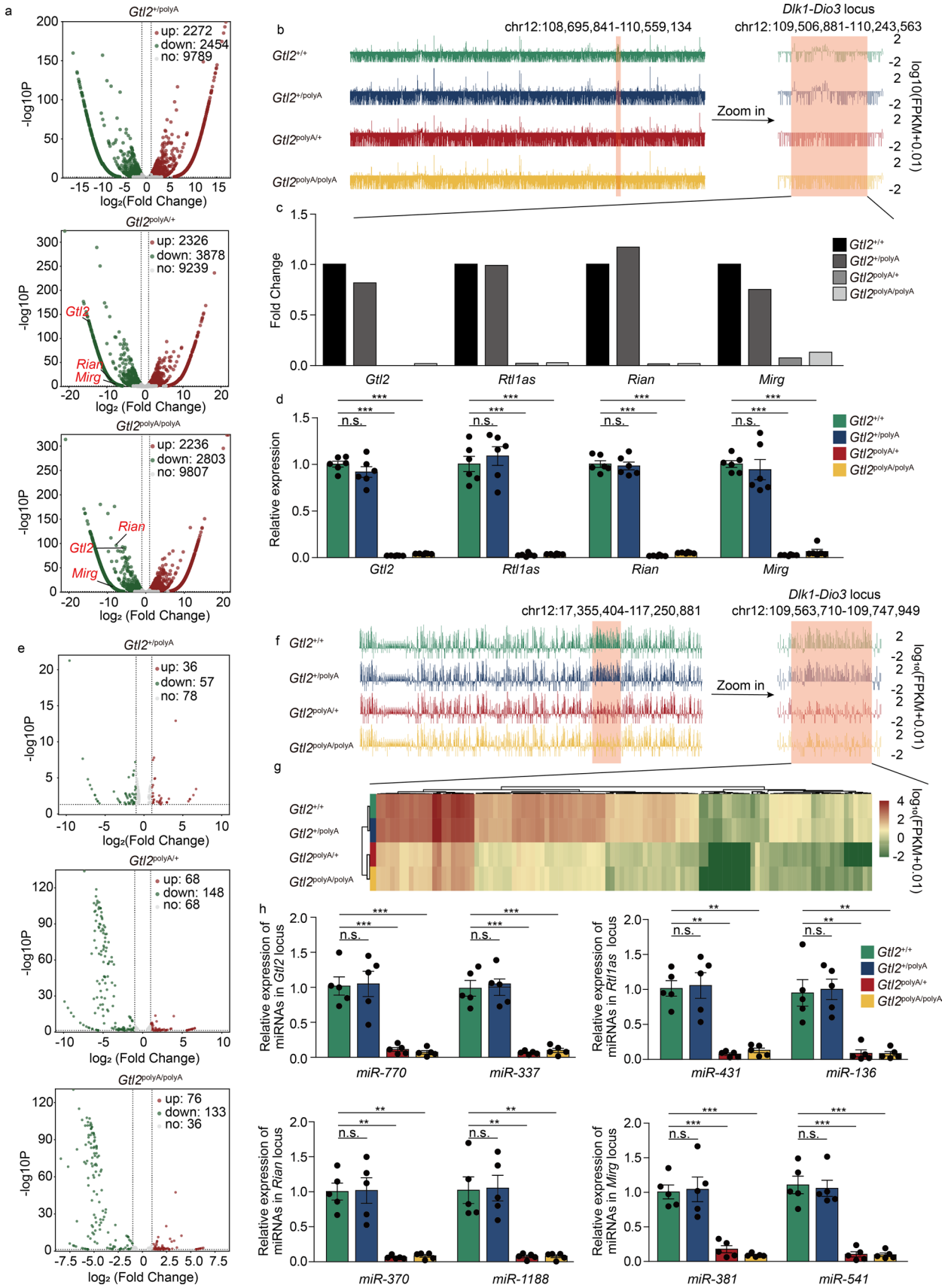
a
Gtl2+/polyA
up: 2272
down: 2454
no: 9789
-log10P
log2(Fold Change)
Gtl2polyA/+
up: 2326
down: 3878
no: 9239
Gtl2
Rian
Mirg
Gtl2polyA/polyA
up: 2236
down: 2803
no: 9807
e
Gtl2+/polyA
up: 36
down: 57
no: 78
Gtl2polyA/+
up: 68
down: 148
no: 68
Gtl2polyA/polyA
up: 76
down: 133
no: 36
b
chr12:108,695,841-110,559,134
Dlk1-Dio3 locus
chr12:109,506,881-110,243,563
Gtl2+/+
Gtl2+/polyA
Gtl2polyA/+
Gtl2polyA/polyA
Zoom in
log10(FPKM+0.01)
c
Fold Change
Gtl2
Rtl1as
Rian
Mirg
d
Relative expression
n.s.
f
chr12:17,355,404-117,250,881
Dlk1-Dio3 locus
chr12:109,563,710-109,747,949
g
h
Relative expression of miRNAs in Gtl2 locus
Relative expression of miRNAs in Rtl1as locus
Relative expression of miRNAs in Rian locus
Relative expression of miRNAs in Mirg locus
miR-770
miR-337
miR-431
miR-136
miR-370
miR-1188
miR-381
miR-541

◂**Fig. 2 Termination of Gtl2 transcription resulted in silencing of the maternally expressed RNA in the Dlk1-Dio3 domain. a** Volcano plot of DElncRNAs in *Gtl2*$^{polyA/+}$ and *Gtl2*$^{polyA/polyA}$ embryos at E12.5. **b** lncRNA-seq of embryos at E12.5. **c** The expression of *Gtl2*, *Rtl1as*, *Rian* and *Mirg* in RNA-seq data. **d** qRT-PCR analysis of *Gtl2*, *Rtl1as*, *Rian* and *Mirg*, *β-actin* was used as an internal control, n = 6 Error bars, ± SEM, Student's t-test, n.s., $p > 0.05$; *, $p < 0.05$; **, $p < 0.01$; ***, $p < 0.001$. **e** Volcano plot of DEmiRNAs in *Gtl2*$^{polyA/+}$ and *Gtl2*$^{polyA/polyA}$. **f** miRNA-seq of embryos at E12.5. **g** The expression of miRNAs in *Dlk1-Dio3* domain in RNA-seq data. **h** qRT-PCR analysis of miRNAs in *Gtl2*, *Rtl1as*, *Rian* and *Mirg* locus, *U6* was used as an internal control, n = 5. Error bars, ± SEM, Student's t-test, n.s., $p > 0.05$; *, $p < 0.05$; **, $p < 0.01$; ***, $p < 0.001$

## Termination of Gtl2 transcription resulted in silencing of the maternally expressed RNAs in the Dlk1-Dio3 domain

We next attempt to elucidate the molecular mechanisms responsible for the above results. To this end, we performed whole transcriptome sequencing in four-genotype embryos at E12.5 and detected 29,158 lncRNAs and 2395 miRNAs (Tab. S2). After excluding genes with that FPKM is 0 in all the four genotypes, we screened out differential expression lncRNAs (DElncRNAs) (Tab. S3) and differential expression miRNAs (DEmiRNAs) (Tab. S4), fold change more than 2.0, and p-value less than 0.05.

Firstly, we identified 2272 upregulated and 2454 downregulated lncRNAs in *Gtl2*$^{+/polyA}$, 2326 upregulated and 3878 downregulated lncRNAs in *Gtl2*$^{polyA/+}$ and 2236 upregulated and 2803 downregulated lncRNAs in *Gtl2*$^{polyA/polyA}$ (Fig. 2a) (Tab. S3). RNA-seq data of all lncRNAs showed that *Gtl2*$^{polyA/+}$and *Gtl2*$^{polyA/polyA}$ had a significant downward trend in *Dlk1-Dio3* domain (Fig. 2b), mainly in *Gtl2*, *Rtl1as* (*miR-127*), *Rian* and *Mirg* (Fig. 2c). The results of qRT-PCR were consistent with the trend of RNA-seq (Fig. 2d), indicating that the termination of *Gtl2* transcription led to the silencing of lncRNA in the domain.

The lncRNAs and miRNAs in the *Dlk1-Dio3* domain constitute a large polycistronic transcription unit, and maternally expressed intergenic transcripts downstream of *Gtl2* are transcribed in the same direction as *Gtl2*, and there is no typical promoter sequence present in this region [5]. Therefore, we guessed that miRNAs in the domain would also be severely affected by the termination of *Gtl2* transcription. We identified 36 upregulated and 57 downregulated miRNAs in *Gtl2*$^{+/polyA}$, 68 upregulated and 148 downregulated miRNAs in *Gtl2*$^{polyA/+}$ and 76 upregulated and 133 downregulated miRNAs in *Gtl2*$^{polyA/polyA}$ (Fig. 2e) (Tab. S4). As most of the downregulated miRNAs were located in the *Dlk1-Dio3* domain in *Gtl2*$^{polyA/+}$ and *Gtl2*$^{polyA/polyA}$ (Fig. 2f), we clustered the miRNAs in the domain and found that the four genotypes could be clearly divided into two groups: the survival group including *Gtl2*$^{+/+}$ and *Gtl2*$^{+/polyA}$, and the death group including *Gtl2*$^{polyA/+}$ and *Gtl2*$^{polyA/polyA}$, among them, the expression of miRNAs in *Gtl2*$^{+/polyA}$ were almost unchanged, while the expression of miRNAs in *Gtl2*$^{polyA/+}$ and *Gtl2*$^{polyA/polyA}$ decreased significantly (Fig. 2g). In *Gtl2*, *Rtl1as*, *Rian* and *Mirg* loci, one miRNA with high expression and one with low expression were selected for qRT-PCR verification, the results were identical to RNA-seq data, indicating that the termination of *Gtl2* transcription led to the silencing of miRNAs in the domain (Fig. 2h). Taken together, these data indicated that our model successfully terminated the transcription of the maternally expressed RNAs in the *Dlk1-Dio3* domain and the termination of embryonic development might be closely related to the silencing of these genes.

## Silencing of maternally expressed RNAs in Dlk1-Dio3 domain results in hemorrhage in embryos

Because platelets undergo activities such as activation and aggregation when injured or bleeding [34], the platelet activation in Kyoto Encyclopedia of Genes and Genomes (KEGG) that appeared in *Gtl2*$^{polyA/+}$ and *Gtl2*$^{polyA/polyA}$, but not in *Gtl2*$^{+/polyA}$, caught our attention (Fig. 3a and S2a) (Tab. S5). Gene Ontology (GO) enrichment analysis revealed that GO terms enriched in both *Gtl2*$^{polyA/+}$ and *Gtl2*$^{polyA/polyA}$, but not in *Gtl2*$^{+/polyA}$, were mainly associated with positive regulation of apoptotic process, embryo development, angiogenesis and wound healing (Fig. 3b and S2b) (Tab. S6). These features are associated with the phenotype of bleeding.

We hypothesized that miRNA changes in the death group may play more roles. Therefore, we found the common DEmiRNAs of *Gtl2*$^{polyA/+}$ and *Gtl2*$^{polyA/polyA}$, and overlapped with the miRNAs in the *Dlk1-Dio3* domain to obtain 95 DEmiRNAs (Fig. 3c). We further analyzed the KEGG and GO of target genes of these 95 DEmiRNAs in *Gtl2*$^{polyA/+}$ and *Gtl2*$^{polyA/polyA}$ (Tab. S4). KEGG enrichment analysis revealed platelet aggregation in both *Gtl2*$^{polyA/+}$ and *Gtl2*$^{polyA/polyA}$ (Fig. 3d and S2c) (Tab. S7). In parallel, activated and aggregated platelets were also identified from cord blood smears of *Gtl2*$^{polyA/+}$ and *Gtl2*$^{polyA/polyA}$ embryos (Fig. 3e). This suggests that bleeding or even injury did occur in *Gtl2*$^{polyA/+}$ and *Gtl2*$^{polyA/polyA}$ embryos. In addition, VEGF signaling pathway also appeared in *Gtl2*$^{polyA/+}$ (Fig. 3e), and combined with the related terms such as angiogenesis that appeared in GO of DElncRNAs (Fig. 3b), we speculated that the termination of maternally expressed RNA transcription may cause some effects on blood vessels. GO enrichment analysis revealed liver development in both *Gtl2*$^{polyA/+}$ and *Gtl2*$^{polyA/polyA}$, but not in *Gtl2*$^{+/polyA}$ (Fig. 3f and S2d) (Tab. S8), and the same term was also appeared in the GO enrichment of lncRNAs (Fig. 3b). Taken together,

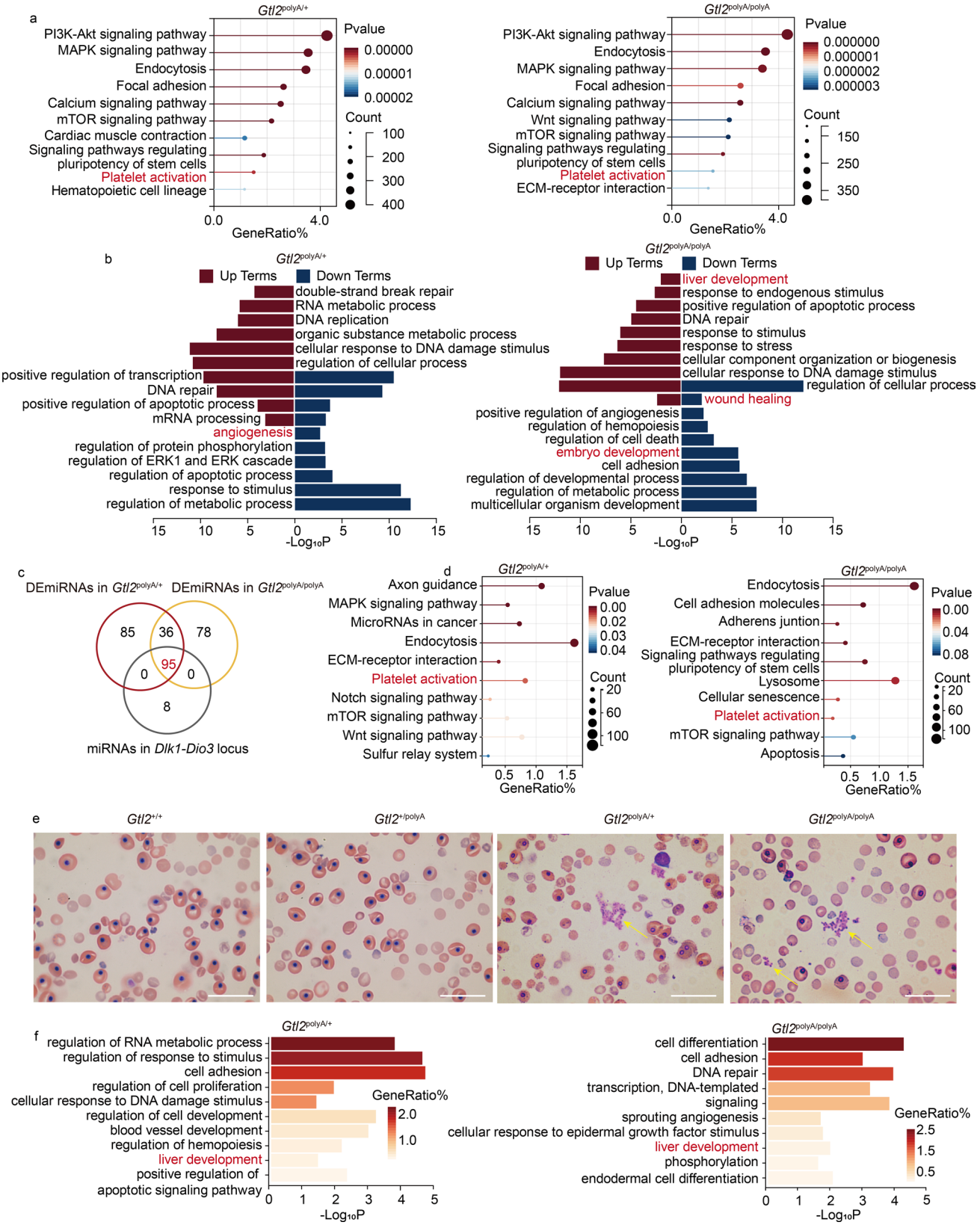
a
Gtl2polyA/+
PI3K-Akt signaling pathway
MAPK signaling pathway
Endocytosis
Focal adhesion
Calcium signaling pathway
mTOR signaling pathway
Cardiac muscle contraction
Signaling pathways regulating pluripotency of stem cells
Platelet activation
Hematopoietic cell lineage
Pvalue
0.00000
0.00001
0.00002
Count
100
200
300
400
0.0
4.0
GeneRatio%
Gtl2polyA/polyA
PI3K-Akt signaling pathway
Endocytosis
MAPK signaling pathway
Focal adhesion
Calcium signaling pathway
Wnt signaling pathway
mTOR signaling pathway
Signaling pathways regulating pluripotency of stem cells
Platelet activation
ECM-receptor interaction
Pvalue
0.000000
0.000001
0.000002
0.000003
Count
150
250
350
0.0
4.0
GeneRatio%
b
Gtl2polyA/+
Up Terms
Down Terms
double-strand break repair
RNA metabolic process
DNA replication
organic substance metabolic process
cellular response to DNA damage stimulus
regulation of cellular process
positive regulation of transcription
DNA repair
positive regulation of apoptotic process
mRNA processing
angiogenesis
regulation of protein phosphorylation
regulation of ERK1 and ERK cascade
regulation of apoptotic process
response to stimulus
regulation of metabolic process
15 10 5 0 5 10 15
-Log10P
Gtl2polyA/polyA
Up Terms
Down Terms
liver development
response to endogenous stimulus
positive regulation of apoptotic process
DNA repair
response to stimulus
response to stress
cellular component organization or biogenesis
cellular response to DNA damage stimulus
regulation of cellular process
wound healing
positive regulation of angiogenesis
regulation of hemopoiesis
regulation of cell death
embryo development
cell adhesion
regulation of developmental process
regulation of metabolic process
multicellular organism development
15 10 5 0 5 10 15
-Log10P
c
DEmiRNAs in Gtl2polyA/+
DEmiRNAs in Gtl2polyA/polyA
85
36
78
95
0
0
8
miRNAs in Dlk1-Dio3 locus
d
Gtl2polyA/+
Axon guidance
MAPK signaling pathway
MicroRNAs in cancer
Endocytosis
ECM-receptor interaction
Platelet activation
Notch signaling pathway
mTOR signaling pathway
Wnt signaling pathway
Sulfur relay system
Pvalue
0.00
0.02
0.03
0.04
Count
20
60
100
0.5 1.0 1.5
GeneRatio%
Gtl2polyA/polyA
Endocytosis
Cell adhesion molecules
Adherens juntion
ECM-receptor interaction
Signaling pathways regulating pluripotency of stem cells
Lysosome
Cellular senescence
Platelet activation
mTOR signaling pathway
Apoptosis
Pvalue
0.00
0.04
0.08
Count
20
60
100
0.5 1.0 1.5
GeneRatio%
e
Gtl2+/+
Gtl2+/polyA
Gtl2polyA/+
Gtl2polyA/polyA
f
Gtl2polyA/+
regulation of RNA metabolic process
regulation of response to stimulus
cell adhesion
regulation of cell proliferation
cellular response to DNA damage stimulus
regulation of cell development
blood vessel development
regulation of hemopoiesis
liver development
positive regulation of apoptotic signaling pathway
GeneRatio%
2.0
1.0
0 1 2 3 4 5
-Log10P
Gtl2polyA/polyA
cell differentiation
cell adhesion
DNA repair
transcription, DNA-templated
signaling
sprouting angiogenesis
cellular response to epidermal growth factor stimulus
liver development
phosphorylation
endodermal cell differentiation
GeneRatio%
2.5
1.5
0.5
0 1 2 3 4 5
-Log10P

◂**Fig. 3 Termination of maternally expressed RNAs in Dlk1-Dio3 domain transcription leads to hemorrhage. a** KEGG analysis of target genes of DElncRNAs in *Gtl2*$^{polyA/+}$ and *Gtl2*$^{polyA/polyA}$ embryos at E12.5. **b** GO analysis of target genes of DElncRNAs in *Gtl2*$^{polyA/+}$ and *Gtl2*$^{polyA/polyA}$ embryos at E12.5. **c** Venn diagram shows the intersection of DEmiRNAs in *Gtl2*$^{polyA/+}$, DEmiRNAs in *Gtl2*$^{polyA/polyA}$, and all miRNAs in *Dlk1-Dio3* domain. **d** KEGG analysis of target genes of DEmiRNAs in *Dlk1-Dio3* domain in *Gtl2*$^{polyA/+}$ and *Gtl2*$^{polyA/polyA}$ embryos at E12.5. **e** Blood smear of peripheral blood at E12.5, yellow arrows point to avtivatee and aggregated platelets, Scale bar, 40 μm. **f** GO analysis of target genes of DEmiRNAs in *Gtl2*$^{polyA/+}$ and *Gtl2*$^{polyA/polyA}$ embryos at E12.5

the DEmiRNAs suggested that the organ affected by ncRNA silencing was the liver.

## Silencing of maternally expressed RNAs in Dlk1-Dio3 domain results in apoptosis

Finally, we identified 249 upregulated and 515 downregulated mRNAs in *Gtl2*$^{+/polyA}$, 609 upregulated and 3147 downregulated mRNAs in *Gtl2*$^{polyA/+}$ and 220 upregulated and 214 downregulated mRNAs in *Gtl2*$^{polyA/polyA}$ (Fig. 4a) (Tab. S9). We found the *Dlk1-Dio3* region in the mRNA profile (Fig. 4b), RNA-seq showed that the expression levels of *Dlk1* and *Rtl1* in *Gtl2*$^{polyA/+}$and *Gtl2*$^{polyA/polyA}$ were 2 times higher than those in *Gtl2*$^{+/+}$, but there was no significant difference between *Gtl2*$^{+/polyA}$ and *Gtl2*$^{+/+}$. The expression levels of *Dio3* in *Gtl2*$^{polyA/polyA}$ were 2 times higher than those in *Gtl2*$^{+/+}$, while the expression level in *Gtl2*$^{+/polyA}$ and *Gtl2*$^{polyA/+}$ was slightly lower than that in *Gtl2*$^{+/+}$, which may account for the lower expression of *Dio3*. (Fig. 4c). The results of qRT-PCR were consistent with the trend of RNA-seq (Fig. 4d), indicating that the termination of transcription of the maternally expressed RNAs in *Dlk1-Dio3* domain activates the expression of the paternally expressed genes.

KEGG enrichment analysis revealed that apoptosis was enriched in DEmRNAs of both *Gtl2*$^{polyA/+}$ and *Gtl2*$^{polyA/polyA}$, but not of *Gtl2*$^{+/polyA}$ (Fig. 4e and S3a) (Tab. S10). GO terms enriched in DEmRNAs of both *Gtl2*$^{polyA/+}$ and *Gtl2*$^{polyA/polyA}$ were mainly associated with apoptosis, wound healing, VEGF signaling pathway and platelet aggregation (Fig. 4f and S3b) (Tab. S11). Among them, platelet aggregation was the same as the experimental results of ncRNA enrichment, wound healing and VEGF signaling pathway appeared again, which had to attract our attention and needed further verification.

In addition, apoptosis occurs simultaneously with the above pathways, we speculated that the termination of maternally expressed RNA transcription may cause some effects on blood vessels and hemorrhage, and the relative activity of Caspase 9 in *Gtl2*$^{polyA/+}$ and *Gtl2*$^{polyA/polyA}$ was significantly higher than that in *Gtl2*$^{+/+}$, but there was no significant change in *Gtl2*$^{+/polyA}$ (Fig. 4g). Taken together, these data suggest that silencing of maternally expressed RNAs in *Dlk1-Dio3* domain cause apoptosis, which may be responsible for vascular damage and hemorrhage.

## Silencing of maternally expressed RNAs in Dlk1-Dio3 domain results in vascular damaged and hemorrhage in fetal livers

The GO functional enrichment of the maternally expressed RNA in the interval was concentrated in the liver (Fig. 3b and f), so we speculated that the above phenomenon may be the most obvious in the liver. To determine the effect of silencing the maternally expressed RNAs in the *Dlk1-Dio3* domain on fetal liver, we obtained fetal livers from all four-genotypes at E12.5. It was found that there was no significant change in appearance of the three mutants compared with *Gtl2*$^{+/+}$ (Fig. 5a). Immunofluorescence of Ki67 at E14.5 fetal livers showing that significant cell proliferation occurred in *Gtl2*$^{polyA/+}$ and *Gtl2*$^{polyA/polyA}$, but not in *Gtl2*$^{+/polyA}$ fetal livers (Fig. S4). The above results have shown that the increase in body and fetal liver weight may be due to cell proliferation which was consistent with the results of KEGG and GO enrichment by the ncRNAs. The trend of weight in four-genotype fetal livers was consistent with that of embryos (Fig. 5b). To further observe the changes at the cellular level in the fetal livers, histological analysis showed that there was no significant change between *Gtl2*$^{+/polyA}$ and *Gtl2*$^{+/+}$ (Fig. 5C). The area of blood vessels in the fetal livers of *Gtl2*$^{polyA/+}$ and *Gtl2*$^{polyA/polyA}$ increased, and some blood vessels were damaged (Fig. 5c). At the same time, a variety of cells, such as hepatocytes and endothelial cells, showed suspected apoptosis phenomena such as cell volume reduction, membrane rupture, karyopyknosis and cell fragmentation (Fig. 5c). Single cell suspension of intact liver was prepared for caspase 9 activity detection. The results showed that the relative activities of *Gtl2*$^{polyA/+}$ and *Gtl2*$^{polyA/polyA}$ were more than 2 times higher than that of *Gtl2*$^{+/+}$ (Fig. 5d). TUNEL enabled us to locate apoptosis in fetal livers, which also confirmed the previous speculation that cells in fetal liver did indeed undergo apoptosis (Fig. 5e). Relative fluorescence intensity of TUNEL showed that the apoptosis degree of *Gtl2*$^{polyA/+}$ and *Gtl2*$^{polyA/polyA}$ were significantly higher than that of *Gtl2*$^{+/+}$, which was consistent with the previous results (Fig. 5f). These results suggest that termination transcription of maternally expressed RNA in *Dlk1-Dio3* domain leads to apoptosis in fetal livers.

Next, combined with the previous histological observation of vascular rupture, we further analyzed the blood vessels of the fetal liver. Immunohistochemistry of CD31 was localized to liver endothelial cells and the results showed fragments of endothelial cell apoptosis, which damaged blood vessels and caused erythrocytes to flow out of the damaged blood vessels, resulting in liver hemorrhage, which was consistent with previous histological analysis (Fig. 5g).

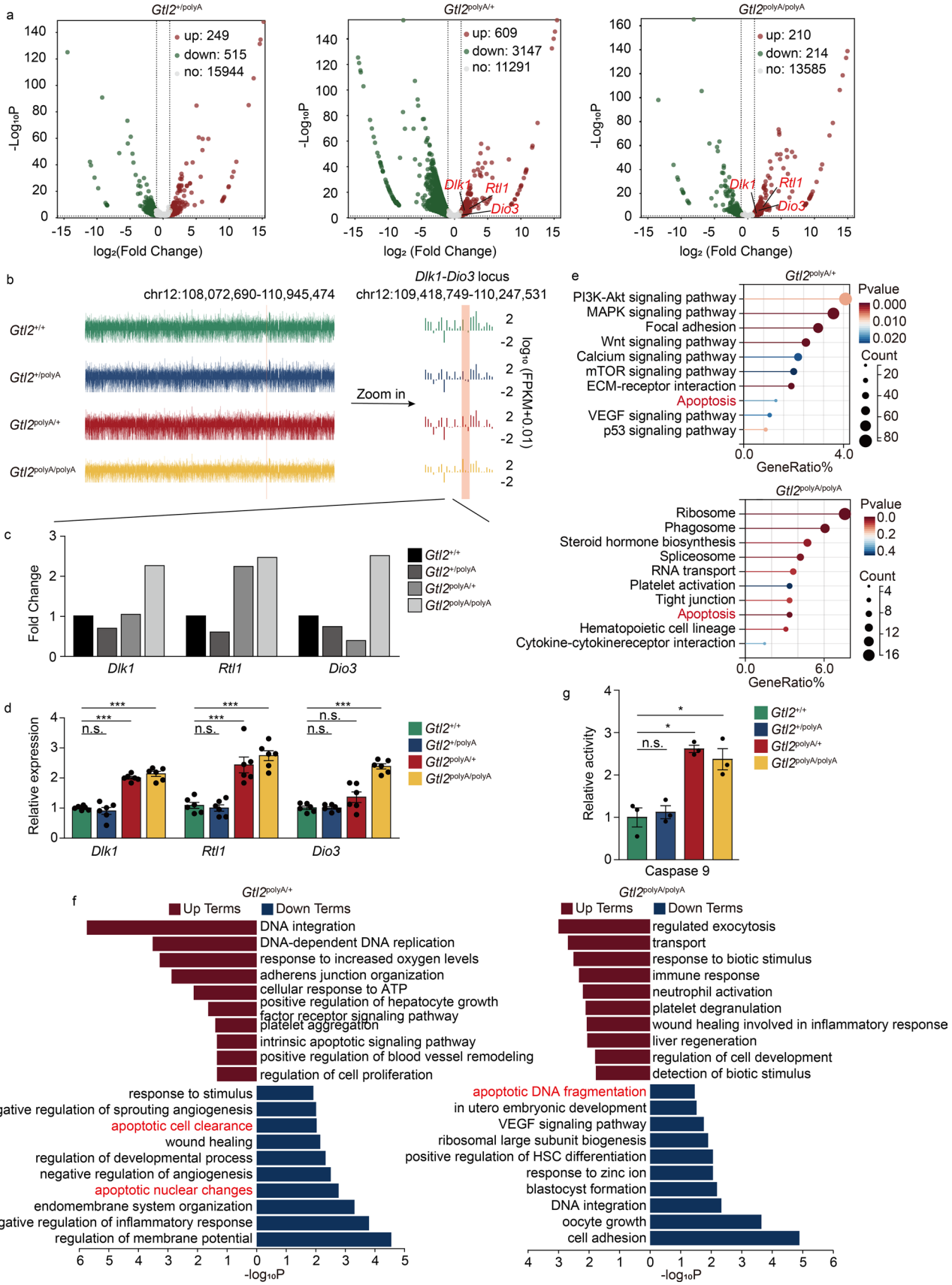
a
Gtl2+/polyA
up: 249
down: 515
no: 15944
Gtl2polyA/+
up: 609
down: 3147
no: 11291
Gtl2polyA/polyA
up: 210
down: 214
no: 13585
-Log10P
log2(Fold Change)
Dlk1
Rtl1
Dio3
b
Dlk1-Dio3 locus
chr12:108,072,690-110,945,474
chr12:109,418,749-110,247,531
Zoom in
log10 (FPKM+0.01)
c
Fold Change
d
Relative expression
n.s.
e
Gtl2polyA/+
PI3K-Akt signaling pathway
MAPK signaling pathway
Focal adhesion
Wnt signaling pathway
Calcium signaling pathway
mTOR signaling pathway
ECM-receptor interaction
Apoptosis
VEGF signaling pathway
p53 signaling pathway
Pvalue
Count
GeneRatio%
Gtl2polyA/polyA
Ribosome
Phagosome
Steroid hormone biosynthesis
Spliceosome
RNA transport
Platelet activation
Tight junction
Apoptosis
Hematopoietic cell lineage
Cytokine-cytokinereceptor interaction
g
Relative activity
Caspase 9
f
Up Terms
Down Terms
DNA integration
DNA-dependent DNA replication
response to increased oxygen levels
adherens junction organization
cellular response to ATP
positive regulation of hepatocyte growth factor receptor signaling pathway
platelet aggregation
intrinsic apoptotic signaling pathway
positive regulation of blood vessel remodeling
regulation of cell proliferation
response to stimulus
negative regulation of sprouting angiogenesis
apoptotic cell clearance
wound healing
regulation of developmental process
negative regulation of angiogenesis
apoptotic nuclear changes
endomembrane system organization
negative regulation of inflammatory response
regulation of membrane potential
-log10P
regulated exocytosis
transport
response to biotic stimulus
immune response
neutrophil activation
platelet degranulation
wound healing involved in inflammatory response
liver regeneration
regulation of cell development
detection of biotic stimulus
apoptotic DNA fragmentation
in utero embryonic development
VEGF signaling pathway
ribosomal large subunit biogenesis
positive regulation of HSC differentiation
response to zinc ion
blastocyst formation
DNA integration
oocyte growth
cell adhesion

◂**Fig. 4 The genetic changes within the Dlk1-Dio3 domain leading to apoptosis. a** Volcano plot of DEmRNAs in $Gtl2^{polyA/+}$ and $Gtl2^{polyA/polyA}$ embryos at E12.5. **b** mRNA-seq of embryos at E12.5. **c** The expression of *Dlk1, Rtl1 and Dio3* in RNA-seq data. **d** qRT-PCR analysis of *Dlk1*, *Rtl1*, and *Dio3*, *β-actin* was used as an internal control, n = 6. Error bars, ± SEM, Student's t-test, n.s., $p > 0.05$; *, $p < 0.05$; **, $p < 0.01$; ***, $p < 0.001$. **e** KEGG analysis of DEmRNAs in $Gtl2^{polyA/+}$ and $Gtl2^{polyA/polyA}$. **f** GO analysis of target genes of DEmRNAs in $Gtl2^{polyA/+}$ and $Gtl2^{polyA/polyA}$. **g** Relative activity of Caspase 9, n = 3. Error bars, ± SEM, Student's t-test, n.s., $p > 0.05$; *, $p < 0.05$

Quantitative analysis of vessel area showed that $Gtl2^{+/polyA}$, $Gtl2^{polyA/+}$ and $Gtl2^{polyA/polyA}$ were 0.98-fold, 1.26-fold and 1.35-fold larger than that of $Gtl2^{+/+}$ (Fig. 5h). The number of blood vessels per square millimeter showed that $Gtl2^{+/polyA}$, $Gtl2^{polyA/+}$ and $Gtl2^{polyA/polyA}$ were 1.03-fold, 0.58-fold and 0.56-fold of $Gtl2^{+/+}$, respectively (Fig. 5i). That is, the average vessel area of $Gtl2^{polyA/+}$ and $Gtl2^{polyA/polyA}$ was significantly larger than that of $Gtl2^{+/+}$, but the number of vessels was significantly less than that of $Gtl2^{+/+}$, and the cause of vascular injury and hepatic hemorrhage was apoptosis of endothelial cells.

## Silencing of maternally expressed RNAs in Dlk1-Dio3 domain had no significant effect on other organs

In order to investigate whether silencing of maternally expressed RNAs in *Dlk1-Dio3* domain has an effect on tissues other than liver, we conducted a further investigation in embryos. Firstly, histological morphology showed that no significant difference, except liver, was observed in the mutant embryo as a whole (Fig. 6a). Secondly, as previous studies have confirmed the effect of maternally expressed RNA silencing in this domain on brain, lung and skeletal muscle [10, 11, 35], we mainly observed these organs (Fig. 6b). We divided the brain into three parts, telencephalon, diencephalon and metencephalon and the results showed that the brain of E12.5 was not fully developed, and there was no significant difference in telencephalon, diencephalon and metencephalon in the mutant (Fig. 6b). The tracheas of all mutants and $Gtl2^{+/+}$ in lung were well developed, and there were some small blood vessels, and the alveoli were not yet formed at this stage (Fig. 6b). There were no significant differences in the bones of the legs, nor any defects in the skeletal muscles (Fig. 6b). It is worth mentioning that our currently published study reported that *Gtl2* transcription termination caused developmental abnormalities in the heart caused by slow proliferation of epicardial cells (Fig. 6b) [36]. These results suggest that silencing of maternally expressed RNAs transcription in *Dlk1-Dio3* at E12.5 does not have a significant effect on major organs except the liver, and the exploration of the effect on the heart needs to be further improved.

qRT-PCR detected the expression of genes in each organ within the range, and the expression trend of maternally expressed RNA in each organ was basically the same, all of them were significantly down-regulated to almost silence, and the expression of paternally expressed genes, *Dlk1* and *Rtl1*, in brain, heart, liver, lung and leg increased about twice, which is basically the same as that of embryo (Fig. 6c). The changes of *Dio3* in heart and lung were not very obvious, which may be the reason for the low expression of *Dio3* within the two organs (Fig. 6c). We selected *Dlk1* and *Gtl2* as high expression genes from maternally expressed RNA and paternally expressed RNA, respectively, and in situ hybridization showed the same expression as qRT-PCR, and both *Dlk1* and *Gtl2* were highly expressed in liver, but not in other organs (Fig. 6d and S5a, b). Thus, the above results indicate that the changes of genes in major organs in the interval are basically the same as those in the whole embryo, and the effect on the liver is greater than that on the other organs, which needs further observation.

## Silencing of Gtl2, but not Gtl2-DMR and IG-DMR, leads to Dlk1 activation

To explore whether the cause of the phenotype was caused by changes in the gene itself or by the methylation status of the *Gtl2*-DMR and IG-DMR, we found a SNP(A/G) site on *Dlk1* that can distinguish between C57BL/6N(G) and DBA/2J(A). After obtaining the cDNA of the embryo of the female mouse of DBA/2J and the male mouse of C57BL/6N after mating, the cDNA fragment containing the SNP site was sequenced. The expression in *Dlk1* of $Gtl2^{+/+}$ and $Gtl2^{+/polyA}$ was mono-allelic, while the expression of $Gtl2^{polyA/+}$ and $Gtl2^{polyA/polyA}$ was bi-allelic. At the same time, we also tested the offspring obtained by mating male DBA/2J mice with female C57BL/6N mice, and the same conclusion was obtained (Fig. 7a). This means that the silencing of maternally expressed RNAs in *Dlk1-Dio3* cause the imprinting loss of *Dlk1*, although, paternally expressed genes were not edited in the domain, *Dlk1*, *Rtl1* and *Dio3* were still affected, which was also likely to have some impact on embryonic development.

Subsequently, we examined *Gtl2*-DMR and IG-DMR. The lengths of IG-DMR and *Gtl2*-DMR detected in this study were 497 bp and 385 bp, correspondingly. These sequences contained 19 CpG and 2 SNP sites, and 15 CpG and 1 SNP sites in C57BL/6N and DBA/2J hybrids, respectively [11, 34] (Fig. 7b and c). The results shown that both of two DMRs maintained the parental origin specific methylation status in E12.5 embryos (Fig. 7b and c). Taken together, the above data indicated that the variation of paternally expressed genes in the domain were caused by silencing of

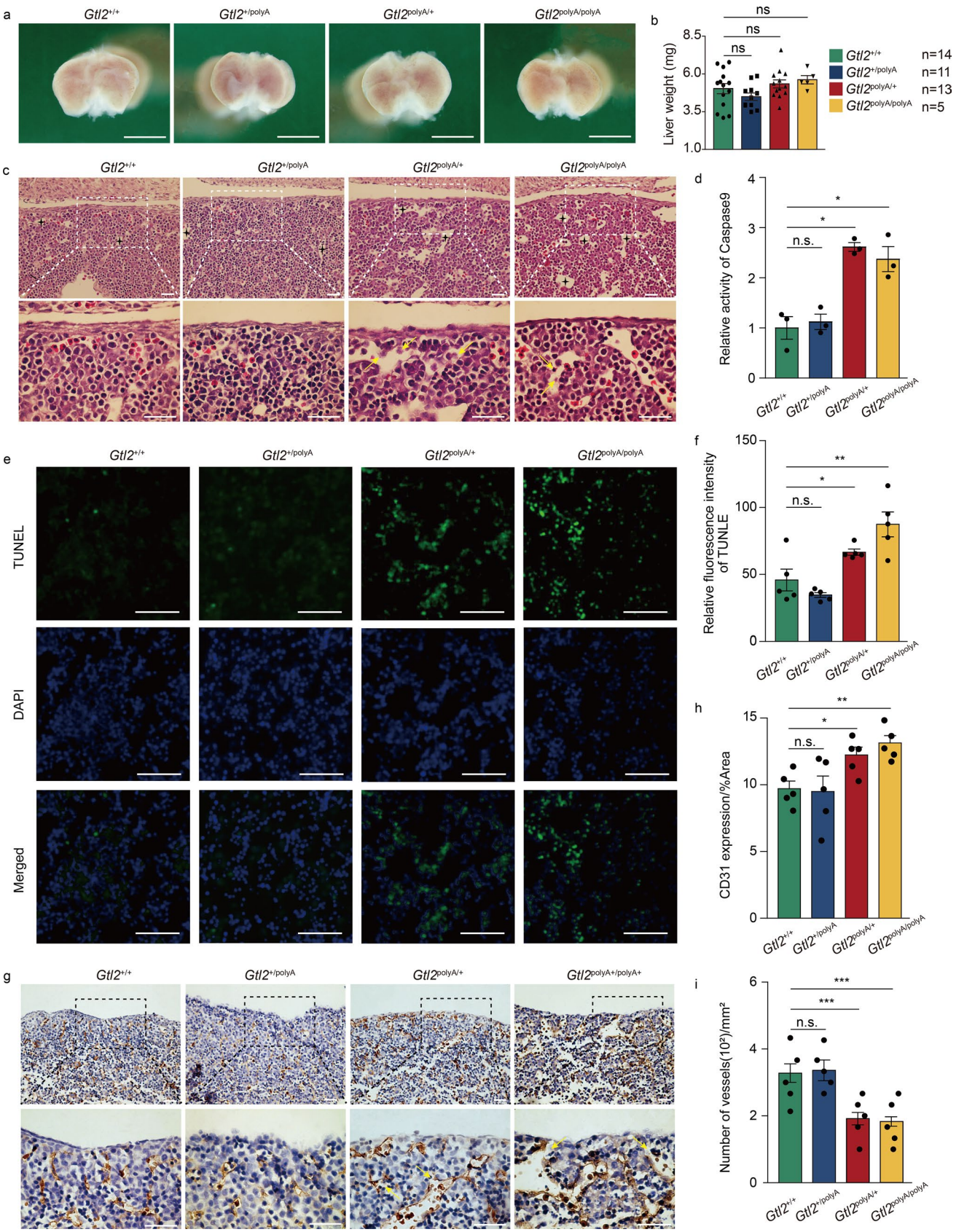
a
Gtl2+/+
Gtl2+/polyA
Gtl2polyA/+
Gtl2polyA/polyA
b
Liver weight (mg)
ns
n=14
n=11
n=13
n=5
c
d
Relative activity of Caspase9
n.s.
e
TUNEL
DAPI
Merged
f
Relative fluorescence intensity of TUNLE
h
CD31 expression/%Area
g
Gtl2polyA+/polyA+
i
Number of vessels(10³)/mm²

◂**Fig. 5 Termination of maternally expressed RNAs in Dlk1-Dio3 domain transcription leads to apoptosis and vascular damage in fetal liver. a** Representative pictures of fetal liver at E12.5. Scale bar, 1 mm. **b** Bar chat showing weight of fetal livers at E12.5, each dot represents a fetal liver. Error bars, ± SEM, Student's t-test, n.s., $p > 0.05$. **c** Representative images of HE staining of fetal livers of each genotype at E12.5. Scale bar, 40 μm. **d** Relative activity of Caspase 9 in fetal liver, n = 3. Error bars, ± SEM, Student's t-test, n.s., $p > 0.05$; *$p < 0.05$. **e** TUNEL fluorescence staining of apoptotic cells in fetal livers, Scale bar, 40 μm. **f** Quantitative analysis of the immunohistochemical staining for TUNEL, n = 5. Error bars, ± SEM, Student's t-test, n.s., $p > 0.05$; *, $p < 0.05$; **, $p < 0.01$. **g** Representative images of immunohistochemistry staining for CD31, apoptosis of endothelial cells are shown as yellow arrows. Scale bar, 40 μm. **h** Quantitative analysis of the immunohistochemical staining for CD31, n = 5. Error bars, ± SEM, Student's t-test, n.s., $p > 0.05$; *, $p < 0.05$; **, $p < 0.01$. **i** Number of blood vessels per square millimeter in each genotype fetal livers, n = 5. Error bars, ± SEM, Student's t-test, n.s., $p > 0.05$; *, $p < 0.05$; **, $p < 0.01$; ***, $p < 0.001$

*Gtl2* rather than by changes in methylation status of *Gtl2*-DMR and IG-DMR.

## Discussion

In this study, we used the improved Easi-CRISPR technique to knock 3 × polyA powerful transcriptional termination sequence into exon1 of *Gtl2*, and finally obtained a mouse model that silenced only the *Gtl2* gene itself without altering other active elements. By using RNA sequencing analysis, we identified that the termination of maternally expressed RNA transcription in the *Dlk1-Dio3* would cause apoptosis of cells in the embryos, especially in the liver, resulting in vascular damage which further caused liver hemorrhage, injury, and finally led to embryonic death.

Previous functional studies of the maternally expressed RNA in the *Dlk1-Dio3* imprinted region have all adopted the method of large deletions of the *Gtl2* gene sequence, which result in the deletion of regulatory elements at the edited locus together [10–12]. Although there was a phenomenon of perinatal death, the cause of death was alveolar dysplasia or skeletal muscle deficiency, which was different from the present study [10, 11]. In addition, other studies have shown that the method of large fragment deletion to study the function of lncRNA will result in false positive results [13, 14]. It has been shown that the insertion of small fragments does not delete any genomic native sequence and does not change staining mass conformation has been proved to be a more effective method for lncRNA study [14, 37]. By inserting the sequence of 3 × poyA to block the expression of maternally expressed RNA in the *Dlk1-Dio3* domain, without deleting other components, the results obtained are more persuasive. Here, we provide a new method to study lncRNA, which can more accurately elucidate the function and regulatory mechanism of the gene itself.

*Gtl2*-induced apoptosis is a type of programmed cell death that occurs after many stimuli, infections, or injuries and plays a key role in physiological processes such as embryogenesis [38]. *Gtl2* down-regulation can regulate FOXO1 and FOXO4 to promote apoptosis through competitive binding of miR-361-5P and miR-23b-3p, respectively [39–41]. Another study found that knockout of *Gtl2* promotes apoptosis of vascular endothelial cells and adipose-derived stem cells by activating the Bcl-2/Bax pathway through the p53 signaling pathway [42, 43]. Deletion *Gtl2* resulted in the down-regulation of lncRNAs and miRNAs in *Dlk1-Dio3* domain, activated the PI3K-mTOR pathway, enhanced metabolic activity, ultimately leading to HSC apoptosis and embryonic death [24]. *MEG3* (or *Gtl2*) inhibited the expression of RASA1 by mediating the histone methylation of the promoter of RASA1 gene by EZH2, thereby activating the RAS-MAPK pathway and enhancing the proliferative and invasive capacities of trophoblasts, and the study suggested that the silent of *MEG3* (or *Gtl2*) maybe a risk fact for unexplained recurrent spontaneous abortion (URSA) [44]. Meanwhile, *Dlk1* acts as an inhibitor of vascular differentiation and inhibits vessel sprouting by antagonizing the NOTCH pathway [45], and it can also play an important role in hematopoiesis and hepatocyte development [46–48]. That means increased dose of *Dlk1* promoted the proliferation of endothelial cells, but inhibited the differentiation of blood vessels, causing the blood vessels in fetal liver to become thicker and fewer (Fig. 5e–g). In addition, it has been reported that *Rtl1* is essential for the maintenance of fetal capillaries, and both its loss and overproduction lead to late fetal and/or neonatal lethality in mice [49]. In addition, our previous study has also shown that maternally expressed RNAs silencing can cause defective narrowing of blood vessels in the placental labyrinth, leading to fetal vascular obstruction and ultimately affecting the exchange function of fetal capillaries [25].

In the process of obtaining embryos, $Gtl2^{polyA/+}$ embryos, but not $Gtl2^{polyA/polyA}$ ones, were found to die at E13.5 (mortality rate was 21.43%), which possibly due to the fact that the $Gtl2^{polyA/+}$ phenotype appeared earlier than $Gtl2^{polyA/polyA}$ embryos. At E12.5, $Gtl2^{polyA/+}$ embryos were in the agonal state, leading to a large change in gene expression. At the same time, although the number of DEGs was smaller in $Gtl2^{polyA/polyA}$ embryos, the changes of gene expression were more significant in *Dlk1-Dio3* region, which may account for the severe mortality after E13.5. We therefore hypothesized that *Gtl2* transcriptional termination may function by regulating different mechanisms in $Gtl2^{polyA/+}$ and $Gtl2^{polyA/polyA}$ embryos. However, this requires a lot of work to confirm. Up to now, there is little information on *Gtl2* transcriptional termination homozygous mice, and most studies have been limited to termination of paternal or maternal transcription [12, 24]. In the future, we will devote ourselves to studying

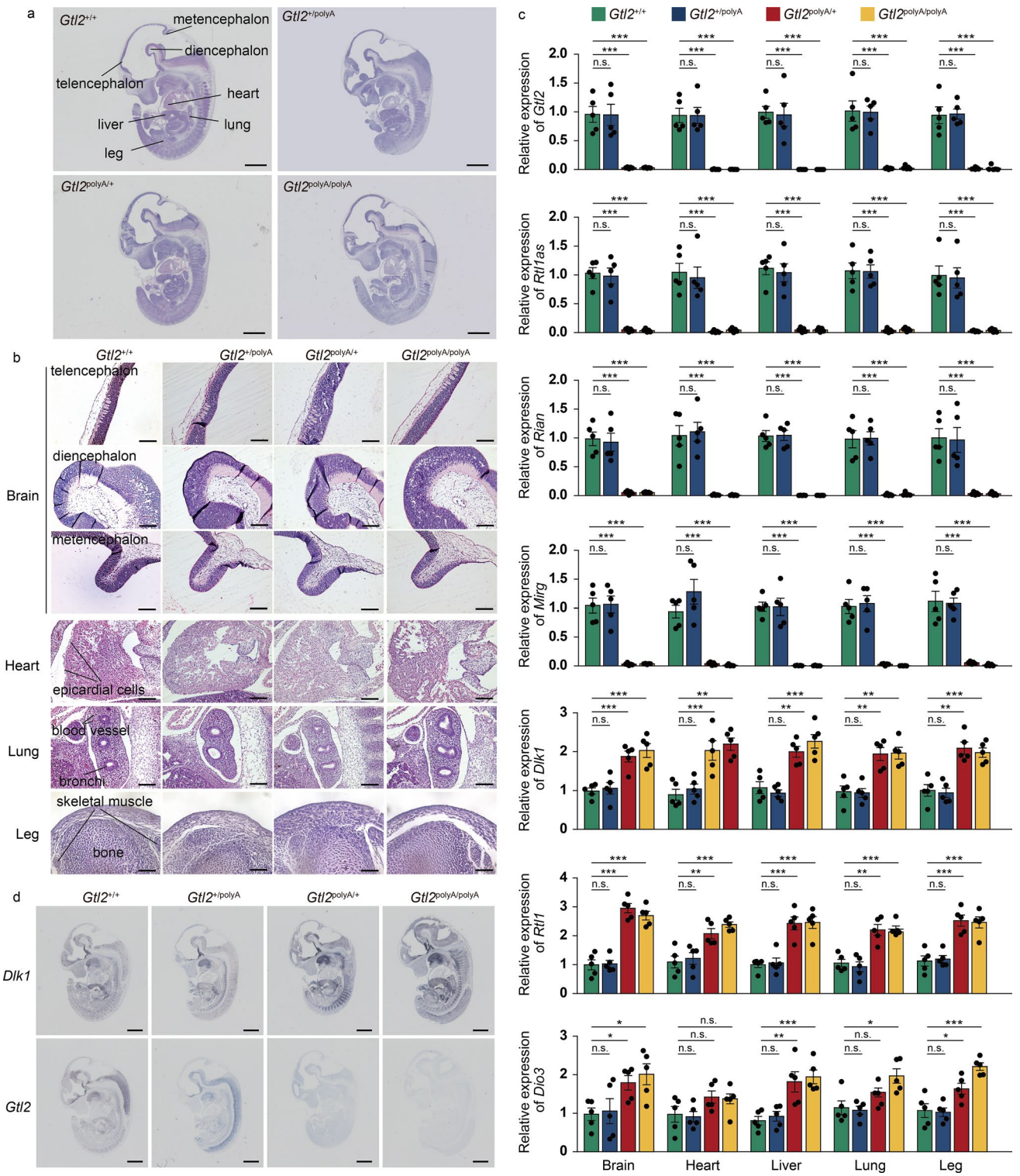


**Fig. 6 Termination of maternally expressed RNAs in Dlk1-Dio3 domain transcription had no significant effect on other embryonic organs. a** Representative images of HE staining of embryos at E12.5. Scale bar, 1 mm. **b** Representative images of HE staining of major organs. Scale bar, 80 μm. **c** qRT-PCR analysis of lncRNAs and mRNAs *in Dlk1-Dio3* domain of major organs, *β-actin* was used as an internal control, n = 5. Error bars, ± SEM, Student's t-test, n.s., $p > 0.05$; *, $p < 0.05$; **, $p < 0.01$; ***, $p < 0.001$. **d** In situ hybridization of *Dlk1* and *Gtl2*. Scale bar, 1 mm

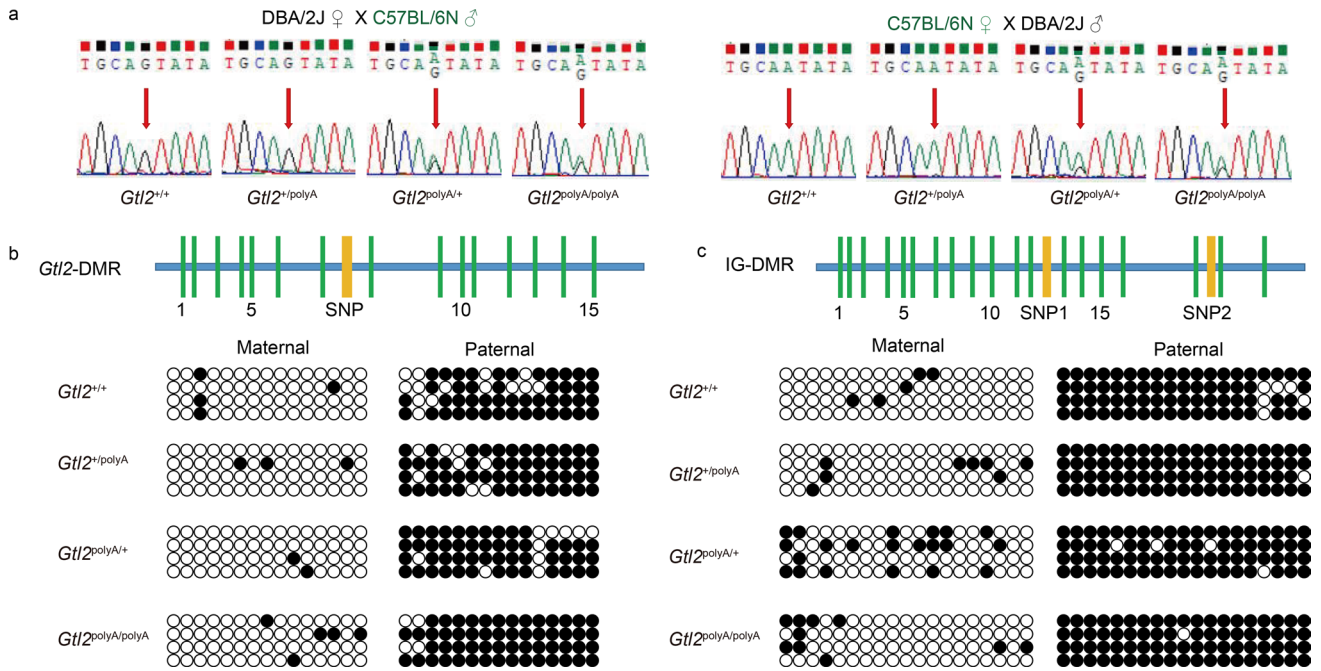


**Fig. 7 Loss of imprinting occurs in Dlk1, which was not caused by Gtl2-DMR and IG-DMR. a** Biallelic expression of *Dlk1* in embryos at E12.5, red arrow points to SNPs. b, c Methylation analysis of *Gtl2*-DMR (**b**) and IG-DMR(**c**). Methylated CpG dinucleotides are represented by filled circles, while unmethylated CpG dinucleotides are represented by open circles

the genetic changes of *Gtl2*$^{polyA/+}$ and *Gtl2*$^{polyA/polyA}$ embryos after E12.5, and give a more comprehensive explanation of this phenomenon through RNA-seq, single-cell RNA-seq, spatial transcriptomics and some other ways.

The *Dlk1-Dio3* imprinted region contains the largest miRNA cluster in the mammalian genome. In this study, our RNA-seq and qRT-PCR data showed that these miRNAs and lncRNAs within the region have the same expression pattern as *Gtl2*, supporting the hypothesis that these ncRNAs act as a large polycistronic transcription unit [6]. Silencing of the maternally expressed ncRNAs in this region reactivate the normally repressed protein-coding genes on the maternal allele, however, the methylation status of IG-DMR and *Gtl2*-DMR remained unchanged, which was consistent with previous reported results [12, 33]. As an enhancer that activates *Gtl2-Rian-Mirg* polycistron, IG-DMR regulates the *Dlk1-Dio3* imprinting domain through *Gtl2*-DMR [12, 50, 51]. *Gtl2*-DMR methylation level are associated with CTCF binding, *Gtl2* expression, and inhibition of paternally expressed genes [33]. However, we detected no change in *Gtl2*-DMR, which may be caused by premature transcriptional termination of *Gtl2*. This also indicates that the *Gtl2* itself plays a role in the inhibition of *Dlk1*. Recent studies have shown that the expression level of imprinted lncRNA was related to the degree of *in-cis* repression, which was related to the formation of lncRNA-protein aggregates [52]. *Gtl2* interact with components of polycomb repressive complexes (PRC) and was thought to be part of this aggregate. However, whether such aggregates form within the *Dlk1-Dio3* interval and how *Gtl2* itself inhibits *Dlk1* in *cis* needs to be further investigated [52–54]. Furthermore, studies have shown that *Gtl2* expression, but not other ncRNAs in the domain, controls inhibition of *Dlk1* [33].

In summary, our study further revealed that transcription termination of the maternally expressed RNAs in the *Dlk1-Dio3* imprinted domain activated the apoptotic and caused severe consequences such as vascular rupture, hepatic hemorrhage and embryonic death, indicating that maternally expressed RNAs in the domain play a crucial role in the regulation of apoptosis and embryogenesis. Although the study has not yet identified the key targets of silencing of maternally expressed RNA in *Dlk1-Dio3* domain in inducing apoptosis, it links the region with vascular and hepatic development, which will be of great significance for the study of embryonic development and even disease occurrence. At the same time, we used Easi-CRISPR method to study the function of lncRNA, which may provide a new way to study the function of lncRNA.

**Supplementary Information** The online version contains supplementary material available at https://doi.org/10.1007/s00018-024-05462-2.

**Acknowledgements** We thank BMKCloud for the analysis of the RNA-seq data. We thank members of our teams for helpful discussion.

**Author contributions** Conceptualization, HRY and QW; Methodology, HRY, XH and ZBH; Validation, ZBH; Formal Analysis, RC and YZ; Resources, XMJZ, XQT, ZYW and BJL; Investigation, MYW and

RC; Writing-Original Draft, HRY; Writing-Review & Editing, MYW, HJH, ZBH, XH, YZ and QW; Visualization, HRY and MYW; Funding Acquisition, YZ and QW.

**Funding** This work was supported by grants from the Key Research and Development Program of Heilongjiang (2023ZX06C09), the State Key Laboratory of Urban Water Resource and Environment of Harbin Institute of Technology (2022TS27), the National Natural Science Foundation of China (U20A20376).

**Data availability** All data supporting this study are available within the article and the Supplementary Materials. The RNA-seq data have been deposited in Gene Expression Omnibus database (GEO) under accession number GSE274171.

## Declarations

**Conflict of interests** The authors declare no competing financial interests.

**Ethics approval and consent to participate** This study was performed in line with the principles of the Declaration of Helsinki. Approval was granted by the Ethics Committee of Harbin Institute of Technology (Date: 19 June 2023 /No: IACUC-2023066).

**Consent for publication** All authors discussed the results and approved the final manuscript.



## References

1. Bartolomei MS (2009) Genomic imprinting: employing and avoiding epigenetic processes. Genes Dev 23:2124–2133. https://doi.org/10.1101/gad.1841409
2. Ferguson-Smith AC (2011) Genomic imprinting: the emergence of an epigenetic paradigm. Nat Rev Genet 12:565–575. https://doi.org/10.1038/nrg3032
3. Enterina JR, Enfield KSS, Anderson C et al (2017) *DLK1-DIO3* imprinted locus deregulation in development, respiratory disease, and cancer. Expert Rev Respir Med 11:749–761. https://doi.org/10.1080/17476348.2017.1355241
4. Sanceau J, Poupel L, Joubel C et al (2024) DLK1/DIO3 locus upregulation by a β-catenin-dependent enhancer drives cell proliferation and liver tumorigenesis. Mol Ther 32:1125–1143. https://doi.org/10.1016/j.ymthe.2024.01.036
5. Rocha STD, Edwards CA, Ito M et al (2008) Genomic imprinting at the mammalian Dlk1-Dio3 domain. Trends Genet 24:306–316. https://doi.org/10.1016/j.tig.2008.03.011
6. Tevendale M, Watkins M, Rasberry C et al (2006) Analysis of mouse conceptuses with uniparental duplication/deficiency for distal chromosome 12: comparison with chromosome 12 uniparental disomy and implications for genomic imprinting. Cytogenet Genome Res 113:215–222. https://doi.org/10.1159/000090835
7. Labialle S, Marty V, Bortolin-Cavaillé M, et al (2014) The miR-379/miR-410 cluster at the imprinted *Dlk1-Dio3* domain controls neonatal metabolic adaptation. The EMBO Journal 33:2216–2230. https://doi.org/10.15252/embj.201387038
8. Royo H, Basyuk E, Marty V et al (2007) Bsr, a Nuclear-retained RNA with Monoallelic Expression. MBoC 18:2817–2827. https://doi.org/10.1091/mbc.e06-10-0920
9. Runte M (2001) The IC-SNURF-SNRPN transcript serves as a host for multiple small nucleolar RNA species and as an antisense RNA for UBE3A. Hum Mol Genet 10:2687–2700. https://doi.org/10.1093/hmg/10.23.2687
10. Takahashi N, Okamoto A, Kobayashi R et al (2009) Deletion of Gtl2, imprinted non-coding RNA, with its differentially methylated region induces lethal parent-origin-dependent defects in mice. Hum Mol Genet 18:1879–1888. https://doi.org/10.1093/hmg/ddp108
11. Zhou Y, Cheunsuchon P, Nakayama Y et al (2010) Activation of paternally expressed genes and perinatal death caused by deletion of the Gtl2 gene. Development 137:2643–2652. https://doi.org/10.1242/dev.045724
12. Zhu W, Botticelli EM, Kery RE et al (2019) Meg3-DMR, not the Meg3 gene, regulates imprinting of the Dlk1-Dio3 locus. Dev Biol 455:10–18. https://doi.org/10.1016/j.ydbio.2019.07.005
13. Goyal A, Myacheva K, Groß M, et al (2016) Challenges of CRISPR/Cas9 applications for long non-coding RNA genes. Nucleic Acids Res gkw883. https://doi.org/10.1093/nar/gkw883
14. Paralkar VR, Taborda CC, Huang P et al (2016) Unlinking an lncRNA from Its Associated cis Element. Mol Cell 62:104–110. https://doi.org/10.1016/j.molcel.2016.02.029
15. Swenson KS, Wang D, Jones AK et al (2023) Metformin Disrupts Signaling and Metabolism in Fetal Hepatocytes. Diabetes 72:1214–1227. https://doi.org/10.2337/db23-0089
16. Perez-Ramirez CA, Nakano H, Law RC et al (2024) Atlas of fetal metabolism during mid-to-late gestation and diabetic pregnancy. Cell 187:204-215.e14. https://doi.org/10.1016/j.cell.2023.11.011
17. Qin K, Lan X, Huang P, et al (2023) Molecular basis of polycomb group protein-mediated fetal hemoglobin repression. Blood blood.2022019578. https://doi.org/10.1182/blood.2022019578
18. Saffarzadeh M, Grunz K, Nguyen TS et al (2020) Macrophage protease-activated receptor 2 regulates fetal liver erythropoiesis in mice. Blood Adv 4:5810–5824. https://doi.org/10.1182/bloodadvances.2020003299
19. Itoh S, Okada H, Koyano K et al (2023) Fetal and neonatal bilirubin metabolism. Front Pediatr 10:1002408. https://doi.org/10.3389/fped.2022.1002408
20. Shao L, Paik NY, Sanborn MA et al (2023) Hematopoietic Jagged1 is a fetal liver niche factor required for functional maturation and engraftment of fetal hematopoietic stem cells. Proc Natl Acad Sci USA 120:e2210058120. https://doi.org/10.1073/pnas.2210058120
21. Yokomizo T, Ideue T, Morino-Koga S et al (2022) Independent origins of fetal liver haematopoietic stem and progenitor cells. Nature 609:779–784. https://doi.org/10.1038/s41586-022-05203-0
22. De Jong IEM, Hunt ML, Chen D et al (2023) A fetal wound healing program after intrauterine bile duct injury may contribute to biliary atresia. J Hepatol 79:1396–1407. https://doi.org/10.1016/j.jhep.2023.08.010
23. Anwar I, Ashfaq UA, Shokat Z (2020) Therapeutic Potential of Umbilical Cord Stem Cells for Liver Regeneration. CSCR 15:219–232. https://doi.org/10.2174/1568026620666200220122536

24. Qian P, He XC, Paulson A et al (2016) The Dlk1-Gtl2 Locus Preserves LT-HSC Function by Inhibiting the PI3K-mTOR Pathway to Restrict Mitochondrial Metabolism. Cell Stem Cell 18:214–228. https://doi.org/10.1016/j.stem.2015.11.001
25. Zhang X, He H, Yu H et al (2024) Maternal RNA transcription in Dlk1-Dio3 domain is critical for proper development of the mouse placental vasculature. Commun Biol 7:363. https://doi.org/10.1038/s42003-024-06038-3
26. Miura H, Quadros RM, Gurumurthy CB, Ohtsuka M (2018) Easi-CRISPR for creating knock-in and conditional knockout mouse models using long ssDNA donors. Nat Protoc 13:195–215. https://doi.org/10.1038/nprot.2017.153
27. Kim D, Langmead B, Salzberg SL (2015) HISAT: a fast spliced aligner with low memory requirements. Nat Methods 12:357–360. https://doi.org/10.1038/nmeth.3317
28. Pertea M, Kim D, Pertea GM et al (2016) Transcript-level expression analysis of RNA-seq experiments with HISAT, StringTie and Ballgown. Nat Protoc 11:1650–1667. https://doi.org/10.1038/nprot.2016.095
29. Robinson MD, McCarthy DJ, Smyth GK (2010) edgeR : a Bioconductor package for differential expression analysis of digital gene expression data. Bioinformatics 26:139–140. https://doi.org/10.1093/bioinformatics/btp616
30. Zhang J, Zhu H, Li L et al (2024) New mechanism of LncRNA: In addition to act as a ceRNA. Non-coding RNA Research 9:1050–1060. https://doi.org/10.1016/j.ncrna.2024.06.002
31. Schnepper AP, Marques LF, Wolf IR et al (2024) Potential global cis and trans regulation of lncRNAs in Saccharomyces cerevisiae subjected to ethanol stress. Gene 920:148521. https://doi.org/10.1016/j.gene.2024.148521
32. Bartel DP (2009) MicroRNAs: Target Recognition and Regulatory Functions. Cell 136:215–233. https://doi.org/10.1016/j.cell.2009.01.002
33. Farhadova S, Ghousein A, Charon F, et al (2024) The long non-coding RNA Meg3 mediates imprinted gene expression during stem cell differentiation. Nucleic Acids Research gkae247. https://doi.org/10.1093/nar/gkae247
34. Wilner GD, Nossel HL, LeRoy EC (1968) Aggregation of platelets by collagen. J Clin Invest 47:2616–2621. https://doi.org/10.1172/JCI105944
35. Martinez ME, Karaczyn A, Wu Z et al (2024) Transgenerational epigenetic self-memory of *Dio3* dosage is associated with *Meg3* methylation and altered growth trajectories and neonatal hormones. Epigenetics 19:2376948. https://doi.org/10.1080/15592294.2024.2376948
36. Teng X, He H, Yu H et al (2024) LncRNAs in the Dlk1-Dio3 Domain Are Essential for Mid-Embryonic Heart Development. IJMS 25:8184. https://doi.org/10.3390/ijms25158184
37. Anderson KM, Anderson DM, McAnally JR et al (2016) Transcription of the non-coding RNA upperhand controls Hand2 expression and heart development. Nature 539:433–436. https://doi.org/10.1038/nature20128
38. Morana O, Wood W, Gregory CD (2022) The Apoptosis Paradox in Cancer IJMS 23:1328. https://doi.org/10.3390/ijms23031328
39. Tsao CW, Aday AW, Almarzooq ZI, et al (2022) Heart Disease and Stroke Statistics—2022 Update: A Report From the American Heart Association. Circulation 145:. https://doi.org/10.1161/CIR.0000000000001052
40. Wang A, Hu N, Zhang Y et al (2019) MEG3 promotes proliferation and inhibits apoptosis in osteoarthritis chondrocytes by miR-361-5p/FOXO1 axis. BMC Med Genomics 12:201. https://doi.org/10.1186/s12920-019-0649-6
41. Wang X, Li X, Wang Z (2021) lncRNA MEG3 inhibits pituitary tumor development by participating in cell proliferation, apoptosis and EMT processes. Oncol Rep 45:40. https://doi.org/10.3892/or.2021.7991
42. Shi Y (2020) MEG3 regulates apoptosis of adipose-derived stem cells. Mol Med Report. https://doi.org/10.3892/mmr.2020.11059
43. Yu Y, Kou D, Liu B et al (2020) LncRNA MEG3 contributes to drug resistance in acute myeloid leukemia by positively regulating ALG9 through sponging miR-155. Int J Lab Hematology 42:464–472. https://doi.org/10.1111/ijlh.13225
44. Zhang J, Liu X, Gao Y (2021) The long noncoding RNA MEG3 regulates Ras-MAPK pathway through RASA1 in trophoblast and is associated with unexplained recurrent spontaneous abortion. Mol Med 27:70. https://doi.org/10.1186/s10020-021-00337-9
45. Huang C-C, Kuo H-M, Wu P-C et al (2018) Soluble delta-like 1 homolog (DLK1) stimulates angiogenesis through Notch1/Akt/eNOS signaling in endothelial cells. Angiogenesis 21:299–312. https://doi.org/10.1007/s10456-018-9596-7
46. Li L, Forman SJ, Bhatia R (2005) Expression of DLK1 in hematopoietic cells results in inhibition of differentiation and proliferation. Oncogene 24:4472–4476. https://doi.org/10.1038/sj.onc.1208637
47. Persson-Augner D, Lee Y-W, Tovar S et al (2014) Delta-Like 1 Homologue (DLK1) Protein in Neurons of the Arcuate Nucleus That Control Weight Homeostasis and Effect of Fasting on Hypothalamic DLK1 mRNA. Neuroendocrinology 100:209–220. https://doi.org/10.1159/000369069
48. Tanimizu N, Tsujimura T, Takahide K et al (2004) Expression of Dlk/Pref-1 defines a subpopulation in the oval cell compartment of rat liver. Gene Expr Patterns 5:209–218. https://doi.org/10.1016/j.modgep.2004.08.003
49. Balusu S, Horré K, Thrupp N et al (2023) MEG3 activates necroptosis in human neuron xenografts modeling Alzheimer's disease. Science 381:1176–1182. https://doi.org/10.1126/science.abp9556
50. Aronson BE, Scourzic L, Shah V et al (2021) A bipartite element with allele-specific functions safeguards DNA methylation imprints at the Dlk1-Dio3 locus. Dev Cell 56:3052-3065.e5. https://doi.org/10.1016/j.devcel.2021.10.004
51. Hiura H, Komiyama J, Shirai M et al (2007) DNA methylation imprints on the IG-DMR of the *Dlk1 – Gtl2* domain in mouse male germline. FEBS Lett 581:1255–1260. https://doi.org/10.1016/j.febslet.2007.02.034
52. Schertzer MD, Braceros KCA, Starmer J et al (2019) lncRNA-Induced Spread of Polycomb Controlled by Genome Architecture, RNA Abundance, and CpG Island DNA. Mol Cell 75:523-537.e10. https://doi.org/10.1016/j.molcel.2019.05.028
53. Sanli I, Lalevée S, Cammisa M et al (2018) Meg3 Non-coding RNA Expression Controls Imprinting by Preventing Transcriptional Upregulation in cis. Cell Rep 23:337–348. https://doi.org/10.1016/j.celrep.2018.03.044
54. Kaneko S, Bonasio R, Saldaña-Meyer R et al (2014) Interactions between JARID2 and Noncoding RNAs Regulate PRC2 Recruitment to Chromatin. Mol Cell 53:290–300. https://doi.org/10.1016/j.molcel.2013.11.012